

Federation University ResearchOnline

<https://researchonline.federation.edu.au>

Copyright Notice

This is the peer-reviewed version of the following article:

Alshareef, A., Shah, R., & Mithulanathan, N. (2020). Impact of PV Plant and Load Models on System Strength and Voltage Recovery of Power Systems. 2020 2nd International Conference on Smart Power & Internet Energy Systems (SPIES), 263–268.

<https://doi.org/10.1109/SPIES48661.2020.9243000>

Copyright © 2020 IEEE. Personal use of this material is permitted. Permission from IEEE must be obtained for all other uses, in any current or future media, including reprinting/republishing this material for advertising or promotional purposes, creating new collective works, for resale or redistribution to servers or lists, or reuse of any copyrighted component of this work in other works.

See this record in Federation ResearchOnline at:

<https://researchonline.federation.edu.au/vital/access/manager/Index>

Examination of PV Penetration and Load Models on System Strength and Voltage Recovery of Power Systems

Abdulrhman Alshareef
School of Information Technology and
Electrical Engineering
The University of Queensland
St Lucia, QLD 4072, Australia
a.alshareef@uq.net.au

Rakibuzzaman Shah
School of Science Engineering and
Information Technology
Federation University Australia
Mt Helen, VIC 3353, Australia
m.shah@federation.edu.au

N. Mithulananthan
School of Information Technology and
Electrical Engineering
The University of Queensland
St Lucia, QLD 4072, Australia
mithulan@itee.uq.edu.au

Abstract— In recent years, the non-conventional generation sources (i.e., wind, PV, and others) have emerged as excellent alternatives for the traditional synchronous machine for power generation. It is also reported that the so-called system strength may be reduced with high penetration of non-conventional generations (NCGs). A number of methods are used to assess the system strength which may not reflect the interdependency or interactions among various factors affecting system strength. This paper presents a thorough assessment to quantify the implication and interaction of various factors affecting the system strength, where the voltage recovery index has been used as a quantification tool.

Keywords— Load Model, PV Plant, Renewable Energy Integration, Short Circuit Capability, Voltage Recovery Index, Uncertainty Modelling

I. INTRODUCTION

The modern power system is undergoing significant changes with the high penetration of non-conventional generations (NCGs) such as wind, photovoltaic (PV), and others. It has been reported that the incremental penetration of NCGs may alter the dynamic characteristics of the system. Therefore, it would be challenging for power system planners and operators to maintain a secure and reliable supply of electrical power. Although with the advent of power electronic technology, converters may bring benefits to the system, there are issues especially related to voltage stability [1]. The point of common coupling (PCC) of these NCGs are weak, and the voltage regulation issues are likely to occur. This issue would be inevitable in many future power grids due to the lower penetration of synchronous generators (SGs). The fast-dynamic response of NCGs may result in a higher sensitivity of voltage to reactive power. A small change in reactive power may lead to voltage oscillation [2, 3].

Furthermore, the effective impedance as seen from the fault location is increased with the reduction of SGs in the system in an NCG dominated system. Therefore, it reduces the short circuit level. Generally, the terminal voltage of SGs is proportional to the short-circuit current. Unfortunately, most NCGs connected to the system are electronically decoupled, thereby, provide no substantial contribution to short-circuit current [2]. Moreover, the short-circuit current of NCGs is limited by the technical limitation [4]. Therefore, with NCGs prevailing in the system, there is a high risk of voltage instability. In a weak

grid, it is mandatory to mitigate the adverse effect of low system strength on the voltage stability including the operation of existing SGs and NCGs with the adoption of available solutions.

In the past, system strength assessment, i.e., short-circuit ratio (SCR), was used in AC/DC interface [5]. Most recently, SCR is used to assess the implication of the system strength at the PCC of the renewable energy system [6]. These commonly used methods mostly ignored the influence of loads in the system strength. The uncertainty associated with the operating conditions and faults were also ignored. Moreover, the interdependency of the factors related to system strength is not well reported in the literature. Therefore, this research proposed an assessment methodology to quantify the interdependency of various factors related to system strength. The assessment has been conducted in a realistic representative system with high penetration of PV and different loads.

II. THEORETICAL BACKGROUND

A. System Strength Fundamentals

System strength is “an umbrella term for a suite of interrelated factors that together contribute to power system stability” [7]. This is including all classes of power system stability; i.e. frequency, transient, voltage stabilities. This work discusses the system strength from voltage stability point of view. First, The synchronous generator (SG) has a natural coupling with the rest of the power system. It would respond inherently to any event that occurs in the network to cope up with the new operating condition [8]. Therefore, SG injects reactive current with respect to voltage droop sensed by the SG. This reactive current injection received by a particular bus forms the Short Circuit Capacity (SCC) for nominal operating voltage. The bus voltage stiffness to pre-fault value will be higher if the SCC value is high. The informative illustration of this effect has been discussed next using the system in Fig. 1.

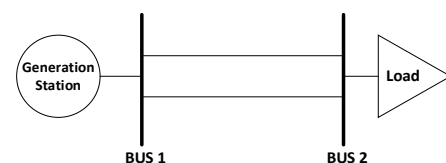


Fig. 1. Simple power system.

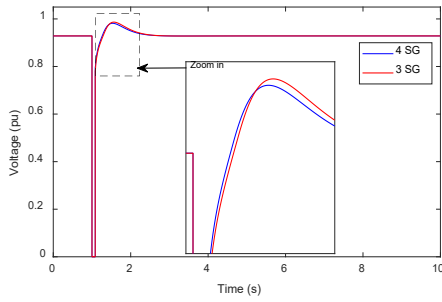


Fig. 2. Voltage responses at bus 2 for three-phase fault.

The RMS time-domain simulation clearly shows that the bus 2 voltage with 4 SGs deviates from the pre-fault voltage narrower than 3 SGs, as depicted in Fig. 2. This is because the SCC is decreased with the reduction of the number of committed generators in the generation station connected to bus 1. It should be worth noting that the SCC provided by SG depends on the MVA rating of the unit [8].

The characteristics and behaviour of large-scale photovoltaic (LSPV) plants are different from SGs. Basically, LSPV plants are converter-based generators or Asynchronous Generators (ASG). Therefore, LSPV plants are entirely decoupled from the grid and mainly depend on control schemes, which is worked as a mediator to enable LSPV plants to react with the operational status of the power system [4, 8]. Understanding of LSPV plants behaviour and reaction to the events in the network would help the system planner and operator to maintain secure operation. Fig. 3 shows typical reactive current injections from SG and LSPV plants that are connected to the transmission station and subjected to a three-phase fault.

The main distinctions of reactive power injection between SG and LSPV are: starting time, ramping, and magnitude of the injected current.

1) *Starting time*: The SG supports the network inherently by injecting reactive current. The electromagnetic coupling between stator and rotor is the reason for this inherent response. However, LSPV needs to be commanded by the control algorithm in order to respond to the changes in the system.

Therefore, This leads to a delay of providing dynamic reactive power support and this delay is not related to the inverters' capabilities, but it is associated with measurements and controller design of the plant [8].

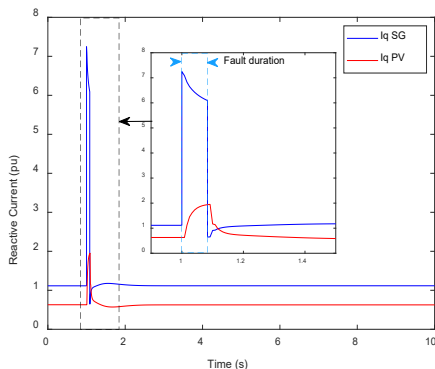


Fig. 3. Typical reactive current response of SG and LSPV.

This reason pushes the regulatory authorities in the industry to state the time response requirement in the standards [9].

2) *Injection ramping*: SG provides reactive injection sooner than LSPV injection as depicted in Fig. 3. The response of LSPV is adjusted and picked neatly to ensure a stable operation of the controller.

3) *Injection magnitude*: The SG can provide reactive current injection up to 6 times the rated current during the fault conditions. However, LSPV reactive current injection is limited up to around 1.2 of the rated current. Moreover, it does not contribute if blocking control mode is activated [10]. This low ceiling level of short circuit contribution is mainly due to power electronics operating limits.

B. Load Model

Load models are widely classified into static and dynamic load models in the power system [11]. In this study, two cases are considered regarding the load model; 100% static load model, and one third (33.33%) of the load as a dynamic load. The description of load models used in this study is given next.

Static load model: The second order polynomial load model as given in (1) and (2) is the frequently used static model in power system studies [11]. However, an elliptical current-voltage characteristic as depicted in Fig. 4 is used to model static load [12]. This load model holds the load MVA as constant until it reaches a certain threshold value, which is 0.7pu in this simulation. When the voltage drops beyond threshold, the load is modified by PSS[®]E software correspondingly.

$$P = P_n \left[p_1 \left(\frac{U}{U_n} \right)^2 + p_2 \left(\frac{U}{U_n} \right) + p_3 \right] \quad (1)$$

$$Q = Q_n \left[q_1 \left(\frac{U}{U_n} \right)^2 + q_2 \left(\frac{U}{U_n} \right) + q_3 \right] \quad (2)$$

The relative participation of constant impedance is represented by parameters p_1 and q_1 , the relative participation of constant current load by p_2 and q_2 and the relative participation of constant power load by p_3 and q_3 .

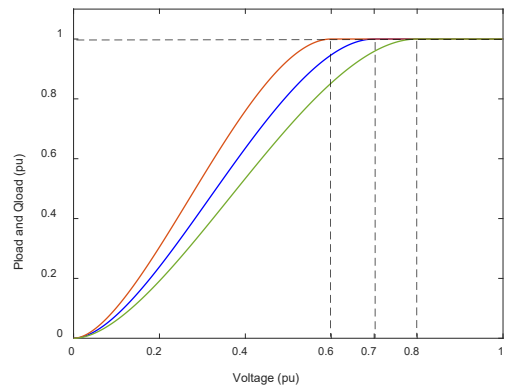


Fig. 4. Constant power load characteristics.

Dynamic load model: The induction motor model including full transient rotor flux dynamics is considered here to

represent the dynamic load model. The motor model is initialized using real power (MW) and terminal voltage to calculate the induction motor slip (S) and reactive power drawn by the motor. The induction motor slip (S) relates the stator and rotor speeds according to:

$$S = \frac{\omega_s - \omega_r}{\omega_s} \quad (3)$$

where ω_s and ω_r are the stator and rotor speeds respectively. The differential equation of rotor acceleration can be expressed as

$$\frac{d\omega_r}{dt} = \frac{1}{2H}(T_e - T_m) \quad (4)$$

where H , T_e , and T_m refer to motor inertia, electrical torque, and mechanical torque, respectively. Fig. 5 is depicted for the equivalent circuit of double-cage induction motor that is used in the analysis to represent the aggregated dynamic loads at transmission level. The used model is named CIM5BL model in PSS[®]E library (PSS/E 2019). Table I shows the model parameters for the induction motor load that are used in this study.

C. Assessment Index

To measure the voltage recovery at each uncertainty set for different penetration levels, voltage recovery index (VRI) is selected as a technical indicator [13]. The VRI compares the voltage recovery according to the pre-fault value. Basically, VRI partitions the voltage into sub-intervals and compares the voltage magnitude of each sub-interval with a ride through criterion starting from fault clear (t_c) time to final observation time (t_f). The WECC ride through criterion is selected for the analysis is shown as:

$$V_{WECC} = \begin{cases} V_1(t) \geq 0.75 & \text{for } t_c \leq t < t_1 \\ V_2(t) \geq 0.80 & \text{for } t_1 \leq t < t_2 \\ V_3(t) \geq 0.95 & \text{for } t_2 \leq t < t_f \end{cases} \quad (5)$$

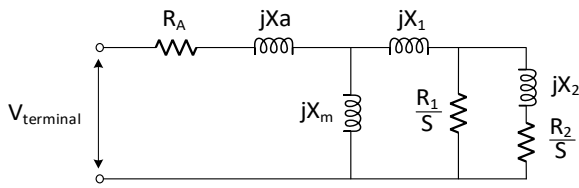


Fig. 5. Equivalent circuit of induction motor.

TABLE I. CIM5BL MODEL PARAMETERS

Parameter	Value (pu)	Parameter	Value (pu)
R _a	0.04	E1	5
X _a	0.277	S(E1)	0.01
X _m	4	E2	7
R ₁	0.04	S(E2)	0.02
X ₁	0.08	PMULT	1.2
R ₂	0.011	H, inertia	0.28
X ₂	0.05	D, damping	2

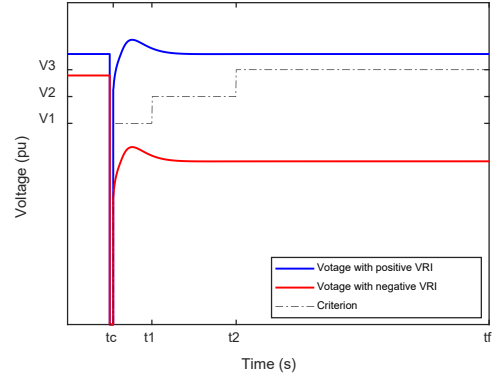


Fig. 6. Voltage recovery with positive and negative VRI.

The mathematical expression of VRI is:

$$VRI = \frac{1}{A} \sum_{j=1}^M \sum_{i=1}^L (\eta_{ji}^+ P_{ji}^{VRI+} + \eta_{ji}^- P_{ji}^{VRI-}) \quad (6)$$

where, A is the total number of samples from fault clear (t_c) time to final time (t_f), M is the number of voltage constraints according to the criterion voltage, and L is the total number of sub-intervals. The term $\eta_{ji}^+ P_{ji}^{VRI+}$ rewards VRI if the voltage recovers upper the voltage criterion and the term $\eta_{ji}^- P_{ji}^{VRI-}$ penalized VRI if the voltage recovers lower the voltage criterion.

The detailed steps and algorithm of VRI calculation are illustrated in [13] and the references therein. It is important to mention here that the VRI value varies between positive one and negative one. However, VRI with negative value indicates unacceptable voltage recovery and vice versa for VRI with positive value as shown in Fig. 6.

III. METHODOLOGY

The steps to evaluate the impact of large-scale PV penetration on the voltage recovery considering the uncertainties of PV output and fault location are shown in Fig. 7. The base case of the test system is modelled in PSS[®]E software including the required dynamic models of the power system components. Suitable probability distribution function (*pdf*) in MATLAB has been used to produce the uncertainty of PV output. However, the fault location is sampled randomly among system buses using a uniformly distributed function in MATLAB. Subsequently, time-domain simulation has been performed by applying a balanced fault for five cycles and the RMS values of voltages are recorded.

System strength is assessed with three different penetration levels (e.g., 20%, 40%, and 60%). The voltage recovery index (VRI) is used as a technical indicator to quantify the system strength. The VRI measures the voltage recovery of the certain bus. However, VRI can be adopted to assess the global voltage recovery of the test system at every single uncertainty set as:

$$VRI_{sys} = \min(VRI_1, VRI_2, \dots, VRI_i) \quad (7)$$

The uncertainty sets for each penetration level are sampled according to the number of large-scale PV plants. Once the assessment of the test network with a static load model is done, the entire process is repeated with one third (33.33%) of the dynamic load model, i.e., induction motors.

IV. SYSTEM MODELLING

A. Test System Model

The test system that has been used in this study is depicted in Fig. 8. It is a reduced order realistic system with 4835 MW load and four thermal generation stations with 30 generator units [14]. The PSS®E library model (GENROU) was implemented for all generator units with governors. All generators are equipped with different types of excitation systems as followings: generation station (Gen_1) contains eight units equipped with IEEE1, Gen_2 contains six units equipped with IEEE Type AC2 exciters, Gen_3 contains nine units equipped with IEEE Type ST2 exciters, and finally, Gen_4 contains seven units equipped with EXPIC1 integral exciters. Three sites, i.e., Bus_2, 3 and 4, are considered to have PV generation. The generators connected to Gen_2, Gen_3, and Gen_4 are de-committed gradually according to PV penetration level. However, station (Gen_1) is kept as the slack bus to maintain the mismatch between load and generation caused by uncertainty in PV output. Table II summarizes the main feature of the test system.

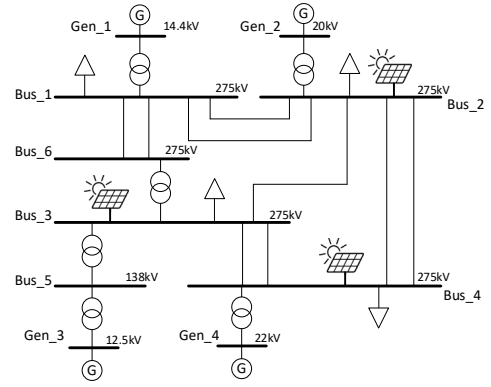


Fig. 8. Reduced order system model.

B. LSPV Model

The WECC generic PV system model is used in this study to represent LSPV plants [15]. The PV plant components are aggregated as a voltage source as given in Fig. 9. The voltage of the PV generation equivalent is stepped up to the voltage of the collector equivalent system. Then, the voltage again raised to the transmission voltage through the main step-up transformer(s).

The PV generator control system contains three renewable energy control models. These are: Generator/Converter (REGC_A) model, Electrical Control (REEC_B) model, and Plant Control (REPC_A) model, all provided by PSS®E models library. The parameters of PV models are verified in [15]. However, Dynamic voltage support (DVS) of LSPV plants is enabled in the study which is aligned with recent utility standards. The LSPV is operated at plant-level control mode. The number of LSPV plants is modelled in the study depends on penetration level and the level of PV penetration calculation is expressed as:

$$PV \text{ Penetration} = \frac{\sum Gen_{PV}}{\sum Gen_{SG} + Gen_{PV}} \quad (8)$$

where Gen_{PV} and Gen_{SG} are the MW output of the PV plants and synchronous generators, respectively.

C. Uncertainty Modelling

Uncertainty is considered in this study for LSPV plant output and fault location. The uncertainty of LSPV output is modelled considering normal distribution with mean (μ) and standard deviation (σ). The standard deviation (σ) is selected to be 10% of μ . Fig. 10 illustrates the variability of PV output at the 20% PV penetration level. The uncertainty of fault location is sampled using a uniformly distributed random function. This means that the probability of fault location among the buses is the same. The MATLAB has been used to model the uncertainties.

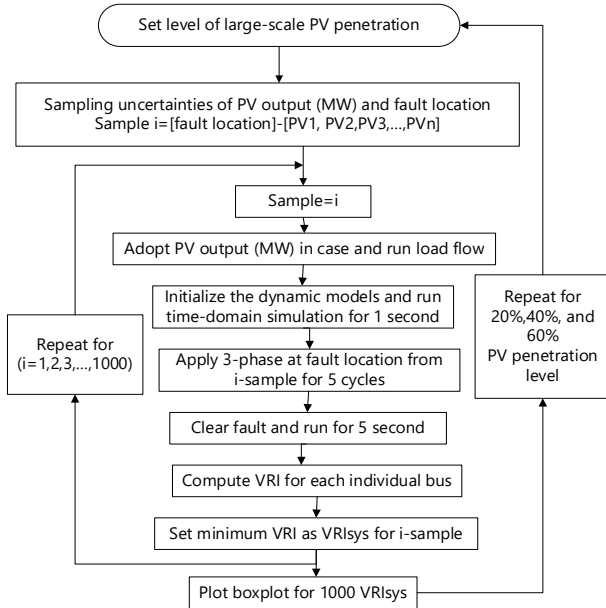


Fig. 7. Methodology flowchart.

TABLE II. MAIN FEATURES OF THE TEST SYSTEM

Station	Rated power (MVA)	No. of machines	AVR model	Gov model
Gen_1	147.5	8	IEEE1	TGOV1
Gen_2	345.0	6	IEEEAC2	IEEEG1
Gen_3	115.5	9	IEEEST2	IEEEG1
Gen_4	455.0	7	EXPIC1	IEEEG1

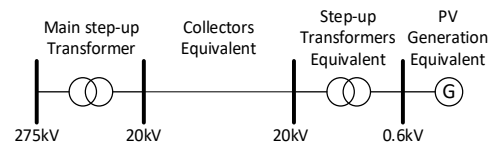


Fig. 9. Single-machine equivalent model of PV plant.

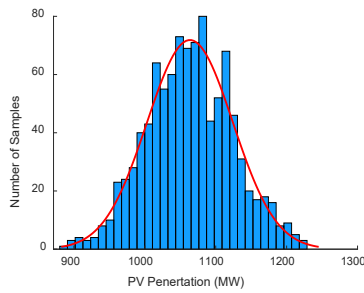


Fig. 10. PV power output variability at 20% penetration level.

V. NUMERICAL RESULTS

Firstly, the explained method in Fig. 7 is applied in these penetration levels with the static loads. Secondly, all simulations are reproduced considering one-third of the dynamic load. These cases are analysed assuming that LSPV is directly connected to the point of integration at the high voltage bus with no transmission line. As a sensitivity analysis, the impact of the overhead transmission line (OHTL) between the point of integration (POI) and LSPV is assessed by varying the transmission line length between 0 to 100km with the step of 20km. The parameter of the transmission line per km is given in Table III. This sensitivity analysis is carried out considering one-third of the dynamic load.

A total of 6000 simulations were performed to investigate the impact of the higher PV penetration on the voltage stability considering the uncertainty of the PV output and fault location. The boxplot of voltage recovery index of the system (VRI_{sys}) shown in Fig. 11 illustrates the influence of LSPV penetration level on the dynamic voltage stability. The VRI has been presented with respect to different LSPV penetration levels and fault locations. Each boxplot represents 1000 simulations and the line in the box points is the median value of VRI_{sys} , while the edges of the boxplot show the upper (75%) and lower (25%) quartile of VRI_{sys} . However, the whiskers demonstrate the variation range of VRI_{sys} corresponding to 99.3% coverage of VRI_{sys} .

TABLE III. TRANSMISSION LINE PARAMETERS PER KM

R (pu)	X (pu)	B (pu)
0.000067	0.000654	0.0025

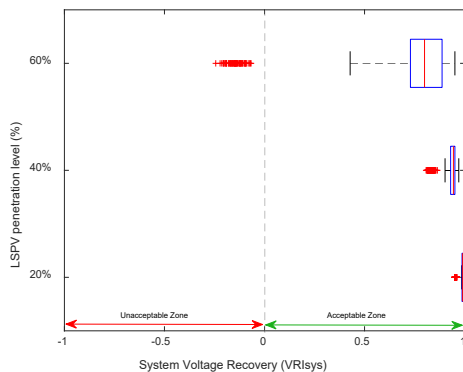


Fig. 11. Boxplots of VRI_{sys} for various penetration levels.

It is clearly observed from Fig. 11 that VRI_{sys} is deteriorated with a higher penetration level. However,

VRI_{sys} is moved further toward unacceptable voltage recovery zone; i.e. $VRI > 0$; with consideration of dynamic load as depicted in Fig. 12. The whiskers of boxplots illustrate the variation range of VRI and that is important to ensure the secure operation of the system and acceptable voltage recovery. For any particular penetration level, VRI_{sys} is improved when the output power of LSPV is sampled at higher value by the uncertainty model. Table IV summarizes the main features of boxplots at Fig. 11 and 12.

Fig. 13 illustrates the impact of adding a transmission line between LSPV and POI for different fault locations. It is observed that the voltage recovery has improved with the increment of length of the transmission. Instead, VRI_{sys} started to decrease with 100km OHTL at 60% penetration level as highlighted in the red circle in Fig. 13. This implies that the charging of OHTL (B in Table III) supports the voltage at POI. However, when PV penetration and line impedance are increased, VRI_{sys} deteriorate rapidly.

VI. CONCLUSION

This paper presented an analysis of system strength considering different PV penetration levels, variability in load models, and faults locations. Instead of using SCR, the voltage recovery index has been used to evaluate the system strength from the voltage stability point of view. It concluded that higher PV penetration is deteriorated the system strength as shown in the voltage recovery pattern. The main reason for this trend is the shrink of reactive power support caused by the replacement of SGs by LSPV plants. Moreover, it is shown that OHTL could help the voltage profile at the network terminal to some extent. However, increasing OHTL length and LSPV capacity will weak the voltage profile.

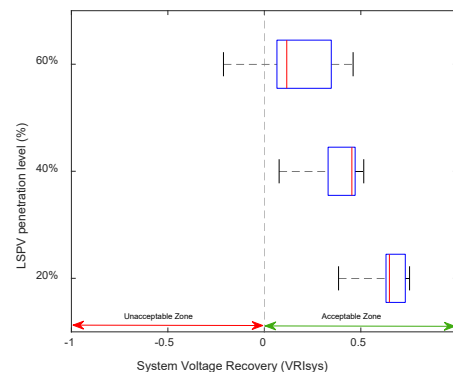


Fig. 12. Boxplots of VRI_{sys} with dynamic load.

TABLE IV. SUMMARY OF BOXPLOTS RESULTS

PV Penetration	Load Model*	Lower Whisker	Median	Upper Whisker
20%	A	0.98556	0.99015	0.99468
	B	0.38457	0.65804	0.75254
40%	A	0.90235	0.94407	0.97092
	B	0.07657	0.43550	0.51512
60%	A	0.42799	0.79981	0.95153
	B	-0.21190	0.11614	0.45996

* A: Static Model, B: 2/3 Static & 1/3 Dynamic

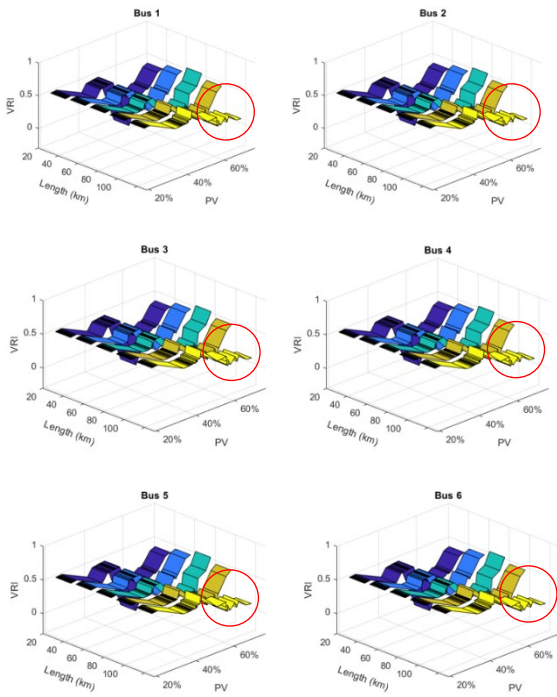


Fig. 13. VRI_{sys} with different fault locations, PV penetrations, OHTL lengths.

REFERENCES

- [1] S. Huang, J. Schmall, J. Conto, J. Adams, Y. Zhang, and C. Carter, "Voltage control challenges on weak grids with high penetration of wind generation: ERCOT experience," in *2012 IEEE Power and Energy Society General Meeting*, 22-26 July 2012 2012, pp. 1-7.
- [2] D. Wu, G. Li, M. Javadi, A. M. Malysheff, M. Hong, and J. N. Jiang, "Assessing Impact of Renewable Energy Integration on System Strength Using Site-Dependent Short Circuit Ratio," *IEEE Transactions on Sustainable Energy*, vol. 9, no. 3, pp. 1072-1080, 2018.
- [3] W. Li, Y. Chun-Jui, H. Min-Han, W. Cheng-Tai, and L. Chieh-Lung, "Analysis of voltage variations and short-circuit ratios of a large-scale offshore wind farm connected to a practical power system," in *2013 IEEE Power & Energy Society General Meeting*, 21-25 July 2013 2013, pp. 1-5.
- [4] D. Wu, M. Javadi, F. Ma, J. Tan, and J. N. Jiang, "A method to identify weak points of interconnection of renewable energy resources," *International Journal of Electrical Power & Energy Systems*, vol. 110, pp. 72-82, 2019.
- [5] H. Urdal, R. Ierna, J. Zhu, C. Ivanov, A. Dahresobh, and D. Rostom, "System strength considerations in a converter dominated power system," *IET Renewable Power Generation*, vol. 9, no. 1, pp. 10-17, 2015.
- [6] S. Grunau, F. W. Fuchs, C.-a.-u. Kiel, and D. Kiel, "Effect of wind-energy power injection into weak grids," in *Proc. EWEA*, 2012, pp. 1-7.
- [7] A. E. M. O. (AEMO), "Power system requirements," 2018.
- [8] F. Milano, F. Dörfler, G. Hug, D. J. Hill, and G. Verbič, "Foundations and Challenges of Low-Inertia Systems (Invited Paper)," in *2018 Power Systems Computation Conference (PSCC)*, 11-15 June 2018 2018, pp. 1-25.
- [9] North American Electric Reliability Corporation (NERC), "Inverter-Based Resource Performance Guideline," September 2018.
- [10] IEEE/NERC Task Force on Short-Circuit and System Performance, "Impact of Inverter Based Generation on Bulk Power System Dynamics and short-Circuit Performance," July 2018 2018.
- [11] A. Adrees and J. Milanović, "Effect of load models on angular and frequency stability of low inertia power networks," *IET*

Generation, Transmission & Distribution, vol. 13, no. 9, pp. 1520-1526, 2019.

- [12] Siemens Industry Inc, "PSS/E Program Operation Manual."
- [13] G. Lammert, D. Premm, L. D. P. Ospina, J. C. Boemer, M. Braun, and T. V. Cutsem, "Control of Photovoltaic Systems for Enhanced Short-Term Voltage Stability and Recovery," *IEEE Transactions on Energy Conversion*, vol. 34, no. 1, pp. 243-254, 2019.
- [14] R. Shah, R. Preece, and M. Barnes, "The Impact of Voltage Regulation of Multiinfeed VSC-HVDC on Power System Stability," *IEEE Transactions on Energy Conversion*, vol. 33, no. 4, pp. 1614-1627, 2018.
- [15] G. Lammert, "Modelling, Control and Stability Analysis of Photovoltaic Systems in Power System Dynamic Studies," 2019.